Saudi Journal of Biological Sciences 28 (2021) 78–89

Contents lists available at ScienceDirect

Saudi Journal of Biological Sciences

journal homepage: www.sciencedirect.com

Original article

Exploring optical spectroscopic techniques and nanomaterials for virus detection

Sello Lebohang Manoto [a,*], Ahmed El-Hussein [b,*,1], Rudzani Malabi [a], Lebogang Thobakgale [a], Saturnin Ombinda-Lemboumba [a], Yasser A. Attia [b], Mohamed A. Kasem [b], Patience Mthunzi-Kufa [a,c]

[a] Council for Scientific and Industrial Research (CSIR), National Laser Centre, P.O. Box 395, Pretoria 0001, South Africa
[b] National Institute of Laser Enhanced Science, Cairo University, Egypt
[c] College of Agriculture, Engineering and Science, School of Chemistry and Physics, University of KwaZulu-Natal, Pietermaritzburg, South Africa

ARTICLE INFO

Article history:
Received 11 June 2020
Revised 7 August 2020
Accepted 23 August 2020
Available online 27 August 2020

Keywords:
Human immunodeficiency virus (HIV)
Anti-HIV gp41 antibodies
Biosensing
Nanomaterials

ABSTRACT

Viral infections pose significant health challenges globally by affecting millions of people worldwide and consequently resulting in a negative impact on both socioeconomic development and health. Corona virus disease 2019 (COVID-19) is a clear example of how a virus can have a global impact in the society and has demonstrated the limitations of detection and diagnostic capabilities globally. Another virus which has posed serious threats to world health is the human immunodeficiency virus (HIV) which is a lentivirus of the retroviridae family responsible for causing acquired immunodeficiency syndrome (AIDS). Even though there has been a significant progress in the HIV biosensing over the past years, there is still a great need for the development of point of care (POC) biosensors that are affordable, robust, portable, easy to use and sensitive enough to provide accurate results to enable clinical decision making. The aim of this study was to present a proof of concept for detecting HIV-1 pseudoviruses by using anti-HIV1 gp41 antibodies as capturing antibodies. In our study, glass substrates were treated with a uniform layer of silane in order to immobilize HIV gp41 antibodies on their surfaces. Thereafter, the HIV pseudovirus was added to the treated substrates followed by addition of anti-HIV gp41 antibodies conjugated to selenium nanoparticle (SeNPs) and gold nanoclusters (AuNCs). The conjugation of SeNPs and AuNCs to anti-HIV gp41 antibodies was characterized using UV–vis spectroscopy, transmission electron microscopy (TEM) and zeta potential while the surface morphology was characterized by fluorescence microscopy, atomic force microscopy (AFM) and Raman spectroscopy. The UV–vis and zeta potential results showed that there was successful conjugation of SeNPs and AuNCs to anti-HIV gp41 antibodies and fluorescence microscopy showed that antibodies immobilized on glass substrates were able to capture intact HIV pseudoviruses. Furthermore, AFM also confirmed the capturing HIV pseudoviruses and we were able to differentiate between substrates with and without the HIV pseudoviruses. Raman spectroscopy confirmed the presence of biomolecules related to HIV and therefore this system has potential in HIV biosensing applications.

1. Introduction

Mankind has battled many types of viruses over the years, which have caused infectious diseases in humans, plants and animals (Zhao et al., 2020). Viruses are the main source of various diseases ranging from mild to life threatening effects with masked or severe symptoms (Virgin, 2014). Different types of viruses have shown to be responsible for the development of certain cancers (Hausen, 2009). Many viruses have resulted in pandemics and a recent example is the corona virus disease 2019 (COVID-19) which started in Wuhan, Hubei province, China in December 2019 and has managed to spread across many countries globally. COVID-19

* Corresponding authors.
E-mail addresses: LManoto@csir.co.za (S.L. Manoto), a.el-husseiny@niles.edu.eg (A. El-Hussein).
[1] Equal contribution to the first author.

Peer review under responsibility of King Saud University.

Production and hosting by Elsevier

https://doi.org/10.1016/j.sjbs.2020.08.034
1319-562X/

is considered a global threat as there is currently no known vaccine or suitable treatment and it is causing thousands of deaths globally with an expected rise unless a safe and effective vaccine and/or treatment(s) are speedily invented. Another virus which can be considered as one of the greatest pandemic in the history of mankind with known dreadful effects worldwide is the human immunodeficiency virus (HIV) (Manoto et al., 2018).

HIV was first discovered at the Pasteur Institute, Paris in 1983 by Luc Montagnier's team and is a causative agent for acquired immune deficiency syndrome (AIDS) (Barre-Sinoussi et al., 1983). According to UNAIDS, there were approximately 37.9 million people living with HIV globally and 770 thousand people died from AIDS related illnesses at the end of 2018 (UNAIDS, 2019). As of end of June 2019, 24.5 million people were receiving antiretroviral therapy (ART) and new HIV infections had significantly reduced by more than 40% since the infection peak in 1997. Sub-Saharan Africa has the highest prevalence of HIV, accounting for more than 70% of all HIV infections (Manoto et al., 2018). Despite, the deep effects and severe impacts of viral infections on the global health and economy, our capabilities for quick, efficient and rapid viral detection are still limited and incomplete. This may be due to many reasons, one of which is the selectivity characteristic of viral infection that could be to specific tissues and/or organs in part due to the differential ability of viruses to infect selected tissues and organ systems (Hausen 2009). The presence of reliable diagnostic tool is an essential for the delivery of proper health services that are needed to the patients and the surrounding communities. In case of the HIV, there is a large number of HIV diagnostics that have been developed. The currently used HIV diagnostics include; western blotting, enzyme linked immunosorbent assay (ELISA) and polymerase chain reaction (PCR). Albeit these techniques have proved to be very reliable and sensitive, identification of the virus and quantification methods are still laboratory based, time consuming and often expensive, this necessitates the need for accurate, rapid and sensitive virus biosensors (Lee et al., 2015).

Biosensors have received a lot of attention for use as point of care (POC) diagnostics over the past few years. Of note, biosensors are seen as a potential and robust tool for the diagnosis of crucial viruses like COVID-19 instead of the time consuming and expensive real-time reverse transcription-polymerase chain reaction (RT-PCR) (Nguyen et al., 2020). The development of biosensors could save thousands of lives on the urge of such severe viral infections by the rapid identification and proper segregation from other uninfected people. The general aim of developing biosensors is to allow accurate, rapid and convenient testing at the POC setting where care of patients is being administered (Sonawane and Nimse, 2016; Manoto et al., 2020). A biosensor is an analytical device that combines a biological recognition component with a transducer for the detection of analytes (Su et al., 2017). The recognition component of the biosensor usually includes enzymes, antibodies, nucleic acids, microorganisms, cells, tissues and biomimetic materials. Regardless of the type of biosensor and the detection of the analyte either at solid-liquid interphase or in a solution involving the use of nanoparticles, the attachment of enzymes, antibodies, DNA or cells is inevitable (Sonawane and Nimse, 2016). Assay sensitivity of biosensors depends on the conformation of the immobilised biomolecules such as antibodies and therefore performance of the system is greatly dependent on the surface chemistry used for immobilisation of biomolecules (Welch et al., 2017).

The introduction of nanotechnology in the biosensor field has increased the sensitivity and other analytical characteristics of the biosensor. Nanotechnology uses nanoparticles ranging between 1 and 1000 nm in size and these particles have unique properties such as surface chemistry, shape dependence and optical properties that enable a variety of application including bioimaging, biosensing, vaccine development and drug delivery (Jazayeri et al., 2016). Various types of nanomaterials such as carbon nanotubes (CNTs), quantum dots, magnetic nanoparticles, selenium nanoparticles (SeNPs), silver (Ag) and gold nanoparticles (AuNPs) or gold nanoclusters (AuNCs) have been used in biosensors with gold particles being the most commonly used type of nanoparticles because of their ability to increase sensitivity and specificity (Zhang et al., 2009).

AuNCs have played a pivotal role in recent advances of fluorescent probe research because of their ability to fluoresce while SeNPs has attracted attention because of their large surface area, high surface activity, powerful adsorbing ability and low toxicity. AuNCs have been used in fields such as biomarkers detection, fluorescence detection and catalysis because of their good stability of fluorescence, low cytotoxicity and good biocompatibility. SeNPs also show favourable biocompatibility and can be easily conjugated with biomolecules without losing activity and preparing them is easy and cost effective (Wang et al., 2019). Biomolecules such as antibodies can be immobilized on both AuNCs and SeNPs either passively through ionic or hydrophobic interactions or covalently through a chemical reaction with a surface group (Finetti et al., 2016).

The aim of the current study is to present as a proof of concept, the development of a biosensor system that would enable for rapid and robust detection of viral threats. The current research focused on HIV-1 pseudoviruses detection by using anti-HIV1 gp41 antibodies as capturing antibodies. A uniform and stable layer of silane was formed on glass substrates using (3-glycidoxypropyl)trime thoxysilane (GPTMS) for covalent attachment of the amine group of the HIV antibodies to the glass substrates. The HIV pseudovirus was added to the substrates, which then bound to the immobilised HIV antibodies. This was followed by the addition of AuNCs and SeNPs conjugated to HIV antibodies, which would bind to the HIV pseudovirus. The surfaces and nanoparticles before and after conjugation were characterised by UV–vis spectroscopy, transmission electron microscopy (TEM), atomic force microscopy (AFM), laser induced fluorescence (LIF) and Raman spectroscopy.

2. Materials and methods

2.1. Materials

Sodium selenite, ascorbic acid, hydrogen peroxide, sulfuric acid, polyvinylpyrrolidone (PVP), sodium borohydride ($NaBH_4$, 95%), hydrogen tetrachloroauratetrihydrate ($HAuCl_4{\cdot}3H_2O$, 99.999%), cetyltrimethylammonium chloride (CTAC), (3-glycidoxypropyl)tri methoxysilane (GPTMS), Dulbecco's Minimal Essential Medium (DMEM) (D5796), fetal bovine serum (FBS, FBS Superior, S0615), 1% Penicillin-Streptomycin (P4333), phosphate buffered saline (D8537) were purchased from Sigma-Aldrich. Human embryonic kidney cells (HEK293 T cells, ATCC CRL 11268) were obtained from the American Type Culture Collection. Anti-HIV gp41 antibody (ab9065), donkey anti-mouse IgG H&L (ab9065) and HIV-1 p24 in vitro SimpleStep ELISA kit (ab218268) were purchased from Abcam while superfect transfection reagent (310305) was purchased from Qiagen.

2.2. Preparation of SeNPs

A modified chemical reduction method was used, where 5 mM of sodium selenite solution was prepared. Ascorbic acid was used as a stock reducing agent at a concentration of 100 mM and the protecting agent, Polyvinylpyrrolidone (PVP) was made up at 0.1% (v/v) concentration. All solvents were dissolved in Milli-Q water at room temperature. Reactants were introduced in the fol-

lowing order: 2.5 ml of PVP was added to 15 ml of sodium selenite and followed by 2.5 ml of ascorbic acid. The solution was mixed under mild stirring rates for 1–2 min, until a deep red clear colour was achieved, this colour demonstrates reaction progression. The prepared SeNPs were conjugated to anti-HIV1 gp41 antibody (Abcam, ab9065) by mixing the SeNPs and anti-HIV1 antibody at a ratio of 1:1 and sonicating the mixture for 40 min. The solution was centrifuged at 2500 rpm for 1 min to remove unbound antibody and the supernatant was discarded. Conjugates were resuspended in 1X phosphate buffered saline (PBS) with a pH of 7.4.

2.3. Preparation of AuNCs

AuNCs were prepared by modifying Attia et al., 2016 method. In brief, 5 ml of 0.2 M cetyltrimethylammonium chloride (CTAC) solution was mixed with 5 ml of 5 mM hydrogen tetrachloroauratetrihydrate ($HAuCl_4$) solution. While stirring the solution, 60 ml of ice-cold freshly prepared 0.1 M sodium borohydride ($NaBH_4$) was added and this resulted in the formation of a solution with a brownish yellow colour. Vigorous stirring of the cluster solution was continued and used after 5 min of preparation. The prepared AuNCs were conjugated to anti-HIV1 gp41 antibody as before.

2.4. UV–vis absorption spectroscopy

The absorption spectra were analysed using the NanoDrop ND 1000 spectrophotometer to determine the red shifts before and after functionalisation of nanoparticles with anti-HIV1 gp41 antibodies. Several UV–vis spectra (~5) were taken for the SeNPs and AuNCs before and after they were conjugated to anti-HIV1 gp41 antibodies.

2.5. Zeta potential measurements

The zeta potential of SeNPs and AuNCs dispersed in water before and after conjugation with anti-HIV1 gp41 antibodies were analysed using the Malvern Zetasizer Nano ZS (Malvern Instruments Ltd., United Kingdom).

2.6. Transmission electron microscopy analysis

Characterisation of SeNPs and AuNCs before and after they were conjugated to anti-HIV1 gp41 antibodies was done using TEM. The samples were prepared by drying a drop of solution containing nanoparticles on the TEM grid. The images of the samples on the grid were taken using the JEOL TEM (JEM 2100F).

2.7. Laser induced fluorescence (LIF)

For LIF measurements, we used a continuous wave (CW) diode pumped solid state laser (DPSS) with 100 mW power and emission wavelength was measured at 405 nm. LIF was used to analyse SeNPs and AuNCs before and after conjugation with anti-HIV gp41 antibodies. The examined samples were in a quartz cuvette of 10 mm thickness and the laser light was delivered by means of an optical fibre. The emitted fluorescence was collected and delivered to a spectrometer (USB2000 FLG Ocean Optics, USA) via another optical fibre placed at 90° to the excitation light. Spectra Suit software (Ocean Optics, USA) was used for acquiring and collecting the data, while spectra analysis was done by using the Origin Lab. software, Version 8 (Souad Elfeky and El-Hussein, 2018; Ahmed et al., 2015).

2.8. Cell culture

Human embryonic kidney cells (HEK293 T cells, ATCC CRL 11268) were used for the production of HIV-1 Env pseudovirus. HEK293 T cells were cultured in Dulbecco's Minimal Essential Medium (DMEM) (Sigma Aldrich, D5796) supplemented with 10% fetal bovine serum (FBS, FBS Superior, S0615) and 1% Penicillin-Streptomycin (Gibco, 15140122). The cells were incubated at 37 °C in 5% CO_2 and 85% humidity until they reached a confluency of 80% which was usually after 2–3 days. After reaching confluency, the cells were then co-transfected with components of HIV-1 in order to produce the HIV pseudoviruses.

2.9. HIV-1 pseudovirus production

The HIV-1 pseudoviruses were produced by transfecting HEK293 T cells using the Superfect transfection reagent (Qiagen, 310305) as described by Lugongolo et al., 2017 and Malabi et al., 2019. Briefly, HEK293 T cells with a total concentration of $3x10^6$ cells were seeded in a T75 flask with 8 μg of env HIV-1 plasmid backbone and 4 μg of HIV-1 Plasmid. The supernatant containing pseudoviruses was harvested after 48 h and filtered with a 0.45 μm filtration system. The concentration of the pseudoviruses was quantified using the HIV-1 p24 in vitro SimpleStep ELISA kit (Abcam, ab218268) (data not shown).

2.10. Preparation of silanized glass substrates

Glass substrates were activated using piranha solution (H_2SO_4: H_2O_2, 7:3 v/v) at 75 °C for 45 min in order to hydroxylate the surface of the glass substrates. After activation, glass substrates were thoroughly washed in ultrapure water and blow dried using nitrogen and placed in an oven to remove any water on the surface. Substrates were then exposed to (3-glycidoxypropyl)trimethoxysilane (GPTMS) at 80 °C in vacuum for 6 h. After silanization, the glass substrates were sonicated in toluene, methanol, and ultrapure water and dried under a stream of nitrogen.

2.11. Immobilization of anti-HIV1 gp41 antibody

Anti-HIV1 gp41 antibodies were immobilized on the silanized glass substrates by incubating the glass substrates with HIV antibodies overnight at 4 °C. After overnight incubation, HIV-1 pseudoviruses at a concentration of 300 pg/ml were added to the surface for 1 h at room temperature, followed by washing with ultra-pure water. Anti-HIV1 gp41 antibodies conjugated to SeNPs and AuNCs were the added to the surface of the substrates.

2.12. Fluorescence staining

Fluorescence staining was done to determine the presence of HIV pseudoviruses on the surface of the substrates. Donkey anti-mouse IgG H&L at a concentration of 15 μg/ml was added to the substrate surface which contained HIV-1 pseudoviruses captured by the anti-HIV1 gp41 antibodies and to the surface which only contained anti-HIV1 gp41 antibodies. The excitation and emission wavelengths of the donkey anti-mouse IgG H&L are $495_{Ex}/519_{Em}$ nm and the fluorescence was visualized using the reflected fluorescence system mounted on the inverted microscope (Wirsam, Olympus® CKX41).

2.13. Atomic force microscopy analysis

The surface morphology of glass substrates coated with anti-HIV1 gp41 antibodies, HIV pseudoviruses, SeNPs and AuNCs conjugated to HIV antibodies were analysed using atomic force micro-

scopy (AFM). The AFM images were captured using a Vecco AFM system (Digital Instruments, USA) using a silicon cantilever tip. The tip has a curvature radius of 10 nm and is n-doped silicon, with a resonance frequency of 204–497 kHz and a force constant of ≈10–130 N/m. The images acquired by the AFM instrument were analysed using the Nanoscope software.

2.14. Raman spectroscopy

An illustration of the custom-built Raman optical setup that was used to perform Raman measurements on the surface of the substrates is shown in Fig. 1. The Raman excitation source was a 527 nm single mode diode laser (Evolution Nd:YLF, diode-pumped, Q-switched) of 1 KHz repetition rate with 5 μs pulse duration. The laser beam was expanded using two lenses telescope (L1 and L2) and delivered to the sample through a 100X microscope objective (NA = 1.25). A dichroic mirror was used to direct the laser beam to the back of the microscope objective lens and remove the Rayleigh scattering. The spot size of the beam at the sample was approximately 1 μm with a power of 10 mW. After passing through a notch filter (to further remove the Rayleigh scattering), the backscattered Raman signal was collected and guided to a spectrograph (Andor Shamrock spectrometer) and a deep cooling CCD camera (Newton, DU9-20P, Andor CCD camera) through an optical fiber. A grating with 1200 g/mm and 500 nm as blazing wavelength was chosen to disperse the Raman signal.

3. Results and discussion

3.1. UV–vis absorption spectroscopy

The nanoparticles conjugated to anti-HIV1 gp41 antibodies were characterised using UV–vis spectroscopy (Fig. 2). The spectrophotometer is able to identify components in a solution based on the unique absorbance characteristic of the components in the solution. The SeNPS and AuNCs showed absorption at wavelengths of ~300 and ~250 nm respectively before conjugation with the anti-HIV1 gp41 antibodies. After conjugation with the antibody there was a reduction in the absorption intensity in both SeNPS and AuNCs. The decrease in the UV–vis spectrum intensity could indicate that successful conjugation of nanoparticles to antibodies was achieved. It is generally accepted that the intensity and absorption peak of the nanoparticles is dependent on the size, shape and agglomeration of the particles (Link and El-Sayed, 2003). Both SeNPs and AuNCs maintained their characteristic band shape after conjugating to biomolecules showing that the nanoparticles did not experience aggregation after binding to biomolecules (Vahdati and Moghadam, 2020). Interestingly, no red shifts were recorded after conjugation to HIV antibodies for both SeNPS and AuNCs which was unexpected since most conjugation of nanoparticles to antibodies results in a red shift. To achieve conjugation of nanoparticles to antibodies, physical and chemical interaction can be used and in this study the physical interaction method was adopted. The physical interaction between the antibodies and nanoparticles depends on three phenomena namely; hydrophobic interaction between the metallic surface and the antibody, ionic attraction between the positively charged antibodies and the negatively charged metallic surface, dative binding between the gold conducting electrons and amino acid sulfur atoms of the antibody (Jazayeri, et al., 2016). Despite some limitation of the physical adsorption method, a study by Puertas et al., 2011 reported excellent orientation of antibodies with this method. There is proof that suggests that the plane of interaction of the antibodies with the metal surface does not have any effects on the antigen binding portion because of the net charge distribution and the asymmetry of the antibody (Oliveira et al., 2019).

3.2. Zeta potential measurements

Zeta potential determination is a significant characterization technique of nanocrystals to estimate the surface charge, which can be employed for understanding the physical stability of nanosuspensions (Jiang et al., 2009). Zeta potential measurements were conducted on SeNPS and AuNCs before and after conjugation with HIV antibodies and the changes in zeta potential are shown in Table 1. The zeta potential of SeNPS and AuNCs showed a positive charge irrespective of the conjugation with HIV antibodies. There was an increase in zeta potential of SeNPs from 35 mV before conjugation to 49.9 mV after conjugation. An increase in zeta potential from 16.8 to 33.7 after conjugation with HIV antibodies was also observed in AuNCs. A zeta potential below −20 mV and above +20 mV indicates that the nanoparticles contained in the solution are physically stable due to electrostatic repulsion of individual particles (El-Naggar et al., 2016). Therefore since both SeNPs and AuNCs showed a zeta potential of more than 20 mV this suggests that they were stable before and after conjugation to HIV antibodies and this could be attributed to the greater electrostatic repulsion between nanoparticles. Yu et al., 2017 also observed an increase in zeta potential to 32.3 mV when AuNCs where conjugated to chitosan oligosaccharide lactate. In the event where a zeta potential has a small value, it can suggest the presence of particle aggregation and flocculation due to the Van der Waals attractive forces which act upon the particles and may result in physical instability (Singhvi, 2019). Nanoparticles with high zeta potential values, between 20 and 40 mV, provide the system stability and are less prone to form aggregates or increase in particle size. However, it should be considered that zeta potential values are not an absolute measurement of nanoparticle stability. Those with positive zeta potential have a long circulating half-life due to the absorption of protein components in the blood. In this study, the zeta potential values for SeNPs increased after binding to the protein based antibody and this attained the conjugate more stability and less aggregation as can be seen in the TEM images.

3.3. Transmission electron microscopy

The nanoparticles morphology was characterised using TEM. Fig. 3 shows TEM images of SeNPs and AuNCs before and after they were conjugated to anti-HIV1 gp41 antibodies. The SeNPs appeared as spherical structures when observed with the TEM while AuNCs appeared as crystalline structures. The morphology of the AuNcs are similar to what was observed by Alonso et al., 2016 after successful synthesis of fluorescent AuNcs for human serum immunoglobulin E determination. The shape and morphology of SeNPs before and after conjugation to HIV antibodies remained similar and this suggests that that the quality and morphology of SeNPs was not affected by conjugation to antibodies. AuNCs also maintained its morphology after conjugating to the antibodies. TEM also confirmed that there was no aggregation of AuNCs and the clusters were well distributed while for SeNPs there were a number of aggregates visible, before and after conjugation with anti-HIV1 antibodies. The average size of SeNPs was 42 nm while AuNCs had an average size of 3 nm. Various characteristics of nanoparticles such as the shape, size, and surface charge have been shown to have a strong influence in their diagnostic efficiency (Jazayeri et al., 2016; El-hussein et al., 2020). The surface area to volume ratio of nanoparticles functions as exquisite scaffolds and can affect its biorecognition and detection reactions. Nanoparticles with an enhanced surface to area to volume ratio enables the nanoparticles to achieve excellent bioimmobilization and signal

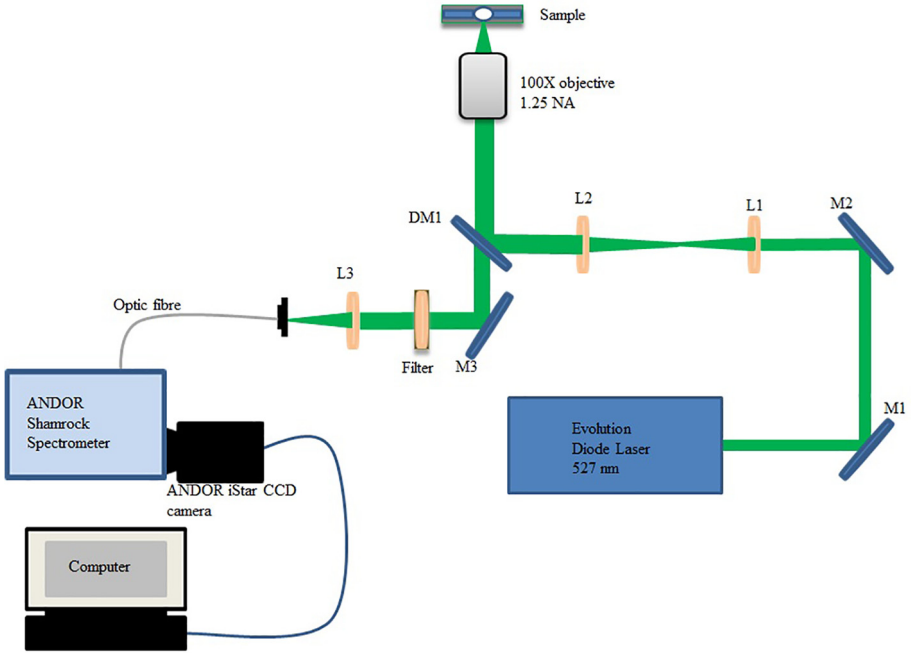

Fig. 1. Illustration of the Raman spectroscopy setup.

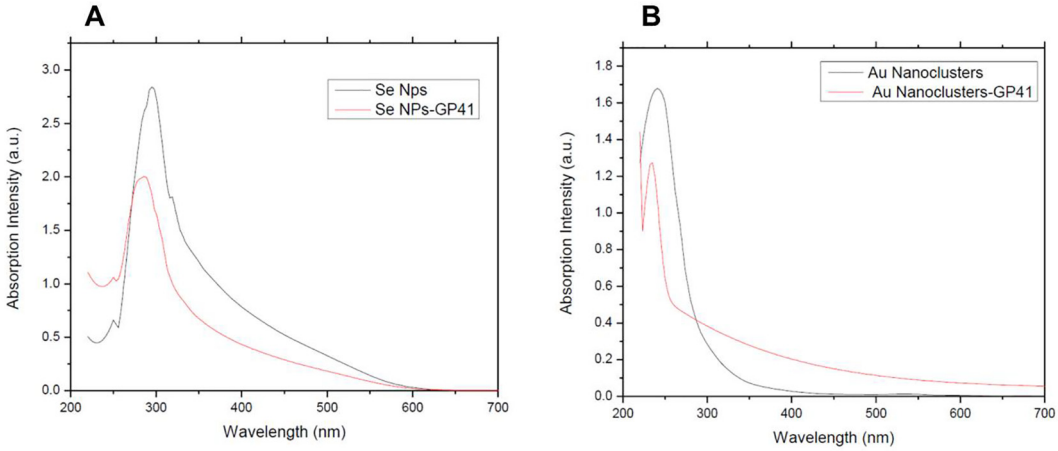

Fig. 2. UV–vis absorption spectra of SeNPs (A) and AuNCs (B) before and after conjugation with anti-HIV1 gp41 antibodies.

Table 1
Zeta potential of selenium nanoparticles and gold nanoclusters before and after conjugation with HIV antibodies.

Nanoparticle type	Un/conjugated	Zeta potential (mV)	Sign of Zeta potential
Selenium nanoparticles	Unconjugated	35 ± 1.7	Positive
	Conjugated	49.9 ± 3.8	Positive
Gold nanoclusters	Unconjugated	16.8 ± 0.8	Positive
	Conjugated	33.7 ± 0	Positive

transduction functions which will result in highly improved specificity and sensitivity for virus detection (Draz and Shafiee, 2018).

3.4. Laser induced fluorescence

The fluorescence spectrum of AuNCs and SeNPs before and after conjugation with HIV antibodies when irradiated with laser light are shown in Fig. 4. Metallic nanoparticles such as gold and semi-metallic elements like selenium have intrinsic fluorescence and a characteristic spectrum. Fig. 4 A revealed how AuNCs are highly fluorescent with peaks at around 450 nm and 500 nm. These fluorescent peaks are still observable for those clusters conjugated with HIV antibodies but broadened and with much less intensity.

There are two main categories for gold nanomaterials, which are gold nanoparticles and nanoclusters. The main differences between the two categories are related to structural and physical properties. The AuNCs are nanomaterials with a size of less than 3 nm. Due to their extreme small size, nanoclusters have unique characteristics and are composed of a dozen to a few hundred atoms (Jin, 2010). Their electronic structures are dependent on their sizes, which match Fermi wavelength based on the fact that the radii of these clusters are inversely proportional to the energy level spacing. Due to the strong quantum confinement of free electrons in the AuNCs, the continuous density of states breaks up into discrete energy levels. This results in size-dependent fluorescence and other attractive molecule properties such as colour tenability and surface tailoring capabilities (Qu et al., 2015). According to

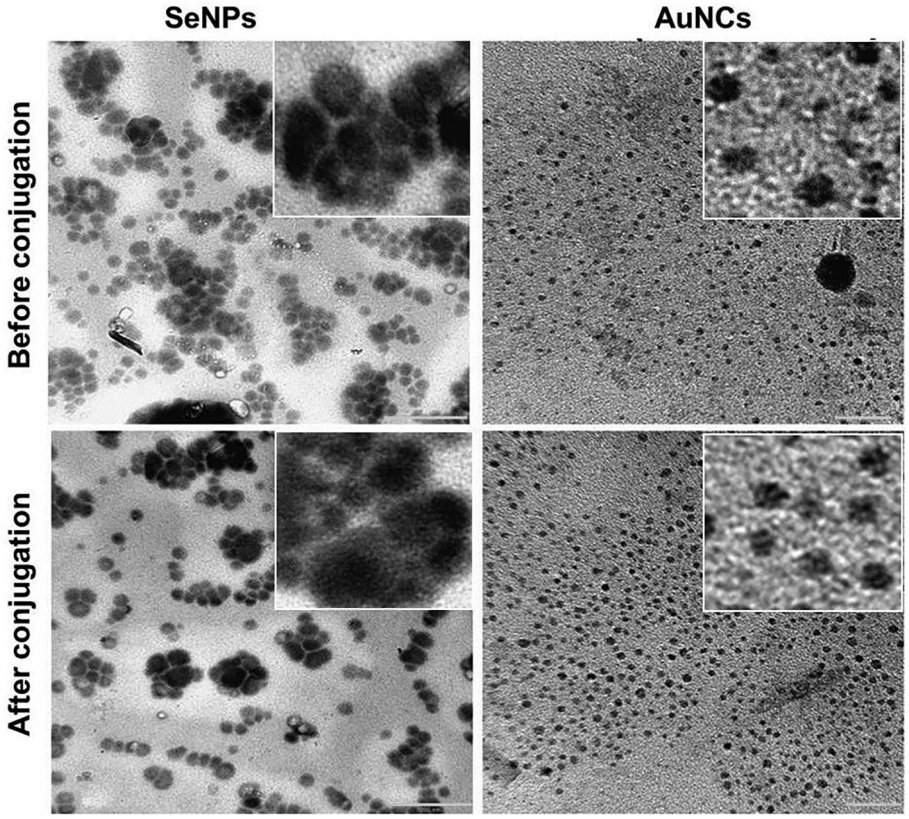

Fig. 3. Transmission electron microscopy (TEM) images of selenium nanoparticles (SeNPs) and gold nanoclusters (AuNCs) before and after conjugation to HIV antibodies. Scale bar for SeNPs denotes 200 nm and 50 nm for AuNCs and the inserts show enlarged picture in the nanoparticles.

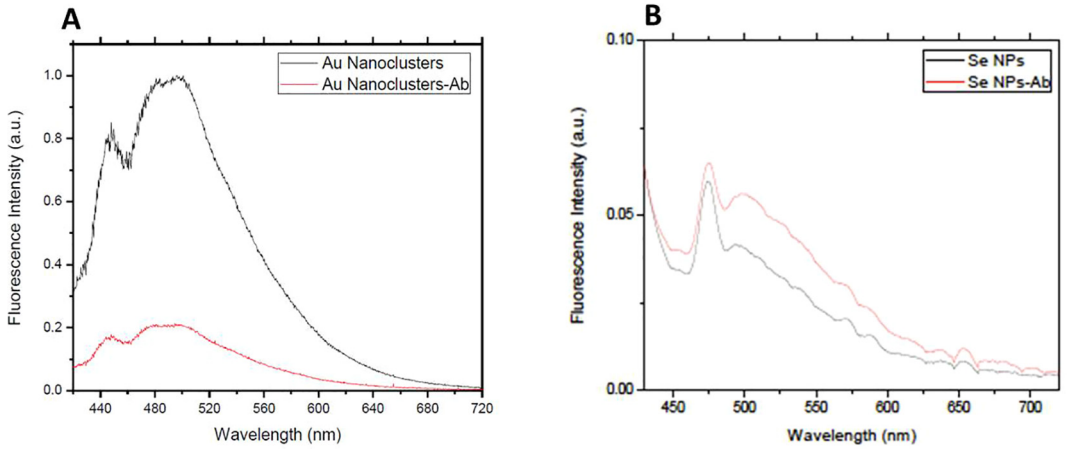

Fig. 4. Fluorescence emission of A: AuNCs alone and after conjugation with anti-HIV gp41 antibodies and B: SeNPs alone and when conjugated to HIV antibodies.

the structural analysis by Wang et al., 2014, the fluorescence characteristic of AuNCs originates from the LUMO-HOMO transition. When fluorophores such as AuNCs absorbs light of a specific wavelength, the fluorophores will then emit energy in a form of fluorescence equalling to the energy variance between the ground state and the excited state. AuNCs are intermediate state between NPs and a single atom and considered as super-atoms or molecular-like species. Moreover, these clusters possess high ratio of surface area to volume, a property that render them suitable for surface functionalization as well as conjugation with biomolecules. Hence AuNCs are potential candidates in various applications like bioimaging and biosensing.

SeNPs on the other hand are shown to have lower fluorescence emission than gold nanoclusters at 475 nm as shown in Fig. 4 B. There is no much difference in the fluorescence pattern between SeNPs and those conjugated with HIV antibodies. This emission spectrum coincides with that reported by Khalid et al., 2016 as they indicated fluorescence emission for SeNPs at 416 and 580 nm. SeNPs have a distinct fluorescence emission in the visible to near infrared region which also makes them ideal for diagnostic applications. However, they are inferior with respect to fluorescence emission when they are compared to AuNCs, because the latter have good photostability, high emission rates and large stokes shift. Of note, Se is a member of the chalcogens family and it is

occurring naturally in the human body for various cellular functions. When Se is in the nanostructure dimensions, it showed to have antimicrobial as well as anticancer activities. Thus, Se NPs are very promising to be used as biosensors as well as in bioimaging tools for both diagnosis and treatment purposes.

3.5. Fluorescence staining

Fluorescence staining was done in order to determine whether the immobilized anti-HIV1 gp41 antibodies on the surface of the glass substrates were able to capture the HIV pseudoviruses. Fig. 5A is an image of donkey anti-mouse IgG H&L added in the presence of HIV-1 pseudoviruses while in Fig. 5B, donkey anti-mouse IgG H&L was added in the absence of HIV-1 pseudoviruses. The donkey anti-mouse IgG H&L reacts specifically with the mouse IgG and with light chains common to other mouse immunoglobulins. Since the glass substrates were treated with mouse IgG antibody (anti-HIV1 gp41 antibodies) it is expected that the donkey anti-mouse IgG H&L will react with the anti-HIV1 gp41 antibodies and show a green fluorescence on the surface of the substrates. This was indeed the observation as shown in Fig. 5B, where donkey anti-mouse IgG H&L was added to the substrates when the virus was not present. This result shows that anti-HIV1 gp41 antibodies were successfully immobilized on the glass substrates and this will enable the antibodies to capture the HIV-1 pseudoviruses. In the presence of the HIV-1 pseudoviruses, no green fluorescence was observed after the addition of donkey anti-mouse IgG H&L. This result suggest that the donkey anti-mouse IgG H&L was not able to react with the anti-HIV1 gp41 antibodies because the latter would have been bound to the HIV-1 pseudoviruses and therefore preventing the binding of donkey anti-mouse IgG to the mouse IgG.

3.6. Atomic force microscopy

AFM was used to analyse the surface of the substrates and each of the scan represent a 2 μm × 2 μm lateral area that was scanned. AFM was used to characterize surfaces that were coated with anti-HIV1 gp41 antibodies followed by the addition of HIV-1 pseudoviruses and no viruses were added to the other substrates as shown in the Fig. 6. Both SeNPs and AuNCs conjugated to HIV antibodies were then added to surfaces and AFM images were taken (Fig. 7). In the absence of HIV-1 pseudoviruses there were fewer complexes that resembled SeNPs and AuNCs as shown in Fig. 7B and C. On the contrary, more structures resembling SeNPs and AuNPs were seen in the presence of HIV-1 pseudoviruses (Fig. 7D and E). Lee et al., 2015 also showed that it was possible to visualize

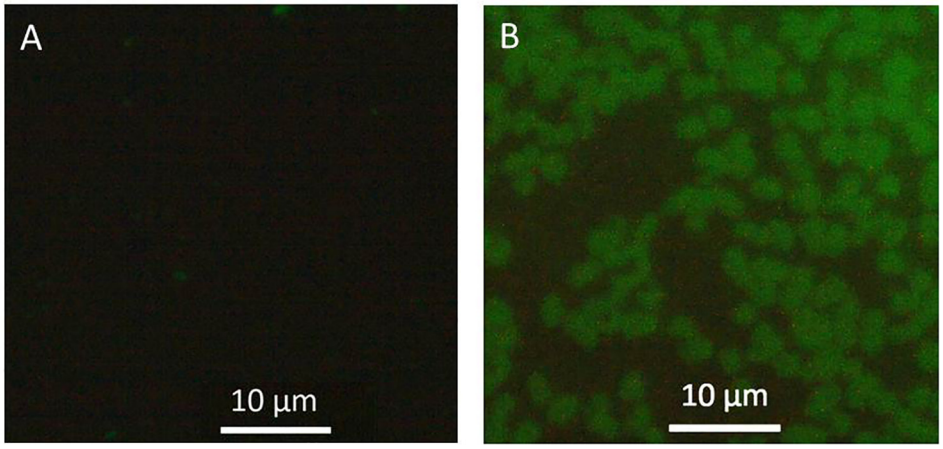

Fig. 5. Fluorescent images of donkey anti-mouse IgG H&L added in the presence (A) and absence (B) of the HIV-1 pseudoviruses.

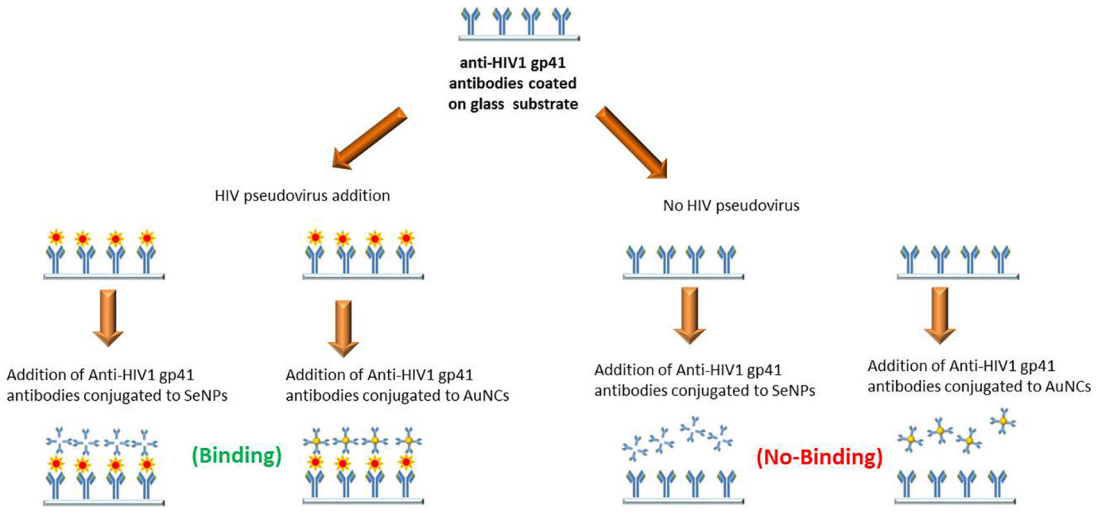

Fig. 6. Illustration of coating anti-HIV1 gp41 antibodies on glass substrates followed by addition or no addition of the HIV-1 pseudoviruses. This is followed by addition of anti-HIV1 gp41 conjugated to SeNPs and AuNPS. In the presence of the HIV pseudovirus both SeNPs and AuNPs binds to the HIV pseudovirus while in the absence of HIV pseudoviruses no binding takes place.

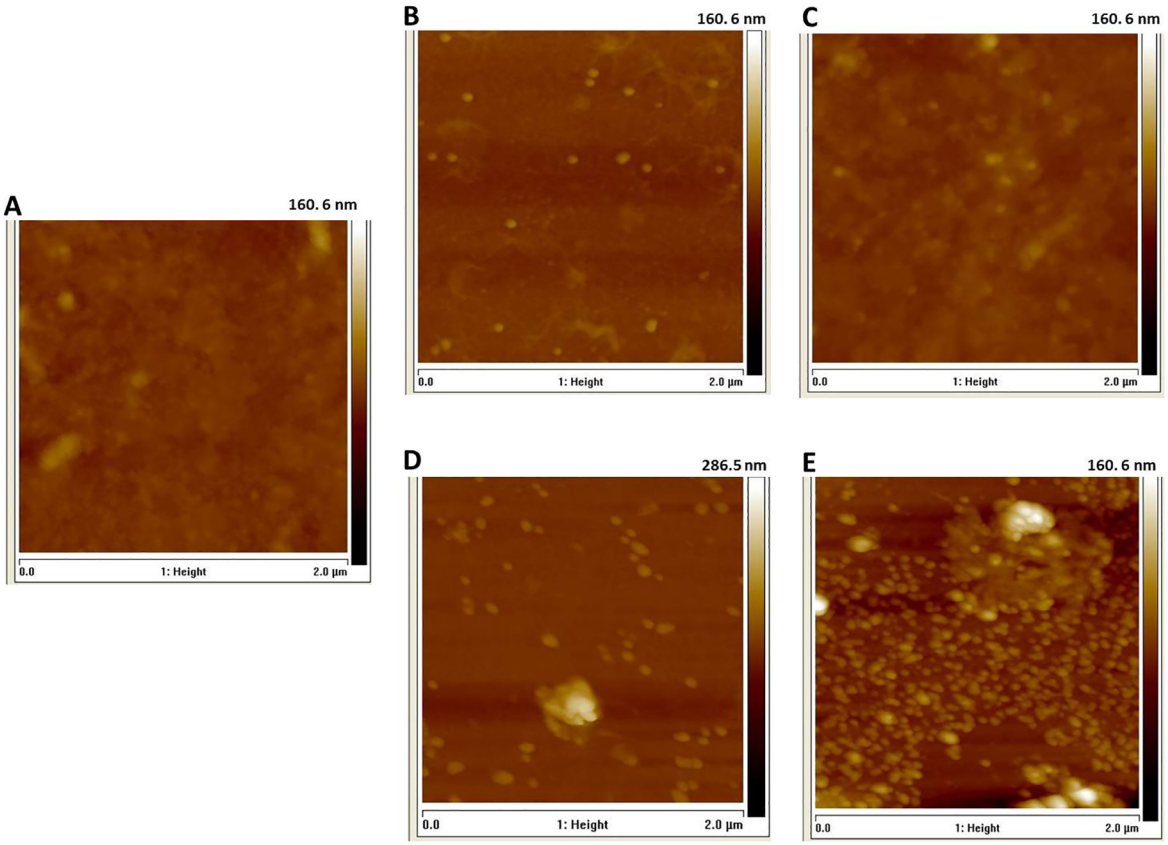

Fig. 7. Atomic force microscopy (AFM) morphologies of glass substrates treated with the anti-HIV gp41 antibodies (A), anti-HIV gp41 antibodies conjugated to SeNPs (B) and AuNCs (C) in the absence of the HIV-1 pseudoviruses. D and E is anti-HIV gp41 antibodies conjugated to SeNPs and AuNCs respectively in the presence of HIV-1 pseudoviruses.

Au nanoparticle-antibody complex due to the presence of Au nanoparticles. The roughness of the surface increased in the surfaces with SeNPs and AuNCs conjugated to HIV antibodies in the presence of the pseudoviruses compared to when there was no HIV pseudoviruses. The root mean square roughness increased by 6 and 2 for SeNPs and AuNPs respectively in the presence of the HIV pseudovirus. This result shows that immobilisation of the HIV antibodies was achieved and the antibodies were able to capture the pseudovirus which bound to SeNPs and AuNCs conjugated to HIV antibodies. The SeNPs had a larger size than AuNPs therefore induced more roughness on the surface.

3.7. Raman spectroscopy

3.7.1. Raman measurement of SeNPs and AuNCS before and after antibody attachments

Raman measurements play an important role in the identification and structural characteristics of molecules, these were measured using a custom built Raman spectroscopy system. The wavelengths of the Raman emission spectrum are characteristic of the light absorbing molecule structure in the sample and the chemical composition, while the intensity of the light scattering is dependent on the concentration of the molecules (Ignat et al., 2010). Fig. 8 shows Raman spectra of SeNPs and AuNCs before and after conjugation to anti-HIV1 gp41 antibodies. The top panel of Fig. 8 shows the spectra of SeNPs (left) and SeNPs conjugated to HIV antibody (right). The SeNPs spectrum shows two vibrations within the region of 200–340 cm^{-1} which is in agreement with the known spectral fingerprint of selenium (Gotoshia and Gotoshia, 2008). Although background subtraction was carried out, carbon-carbon bonds (C-C) which arise from the sample holder were observed due to the enhancement effect from the Se nanomaterials. On the Se-antibody spectrum, the characteristic Se vibrations was reduced significantly in intensity, which suggests conjugation between the nanomaterial and the antibody. Raman effect is a form of inelastic light scattering, where a photon excites the sample and the excitation puts the molecule into a virtual energy state for a short time before the photon is emitted. The inelastic scattering means that the energy of the emitted photon is of either lower or higher energy than the incident photon and after the scattering event, the sample gets into a different rotational or vibrational state (Gardiner and Graves, 1989; Krishnan and Raman,1928). For a molecule to exhibit a Raman effect, there must be a change in its electric dipole-electric dipole polarizability with respect to the vibrational coordinate corresponding to the rovibronic state. The intensity of the Raman scattering is proportional to this polarizability change, therefore, the Raman spectrum (scattering intensity as a function of the frequency shifts) depends on the rovibronic states of the molecule. The binding of the SeNPs to antibodies affects polarization which can be seen by the change of the Se characteristically vibration signals.

The bottom panel of Fig. 8 show AuNCs before (left) and after conjugation (right) with anti-HIV1 gp41 antibodies. The AuNCs before conjugation shows no characteristic Au vibrations however, signal enhancement is observed with the emergence of the aromatic ring vibration found in the polystyrene based sample holder. The AuNCs conjugated to HIV antibody shows characteristics vibration peaks associated with amino acids similar to the Au-antibody spectrum. In the region 500–600 cm^{-1}, disulphide bond (S-S) vibrations are observed. Similarly, vibrations from tryptophan

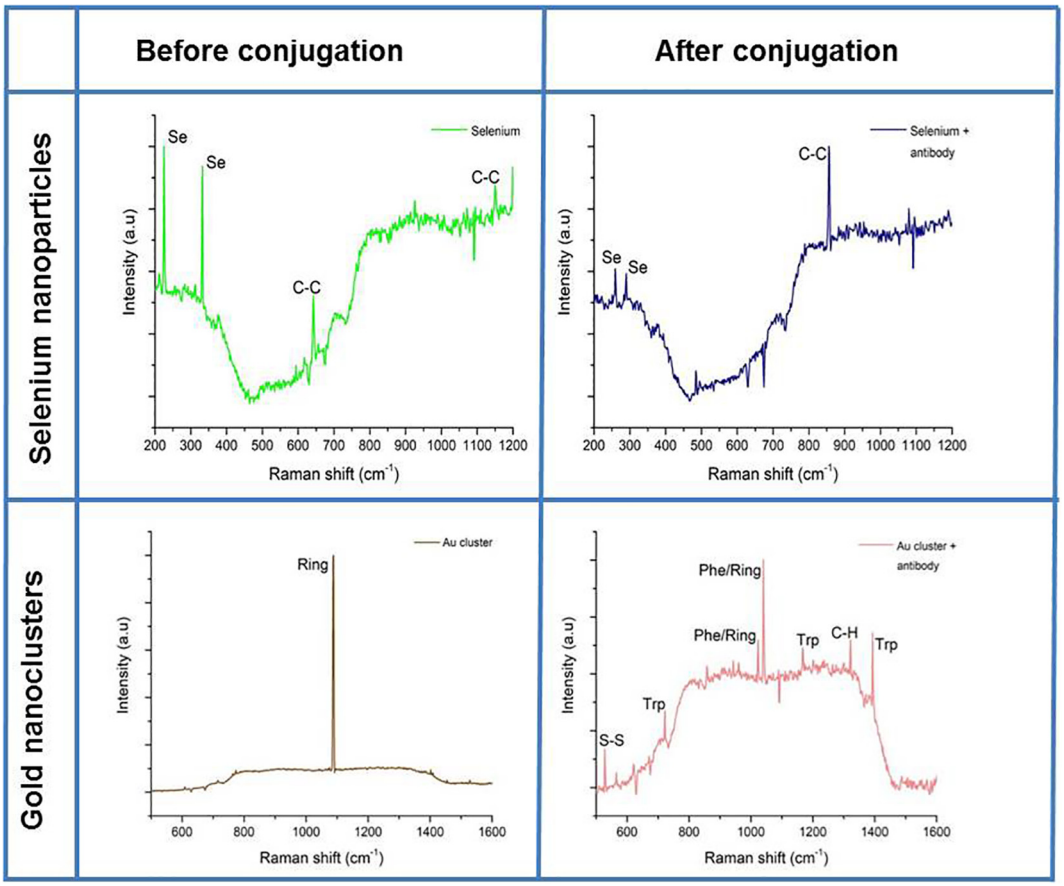

Fig. 8. Raman spectra of SeNPs (top panel) and gold nanoclusters (bottom panel) before and after conjugation to HIV antibody.

(Trp) are seen at in the 700–800 cm^{-1} region. There is a vibration overlap of the amino acid phenylalanine and the aromatic ring of the sample holder in the region 1000–1100 cm^{-1}. The former arises from the conjugation of the AuNCs and the HIV antibody, whereas the latter is a result of the signal enhancement effect of the AuNCs. In the regions 1150–1200 cm^{-1} and 1400–1500 cm^{-1}, vibrations from the Trp are observed, further confirming conjugation between the antibody and AuNcs. Based on the results discussed above, both SeNPs and AuNcs used in this study were able to show significant signal enhancement capabilities. However, Au based substrates were most efficient in producing spectral fingerprints that confirm conjugation between the nanomaterial and the antibody. In comparison to other nanomaterials, metal nanoparticles, particularly AuNPs constitute ideal tools in the diagnostics for a number of reasons, including the ease of surface modification, excellent stability and exceptionally high absorption coefficients (Draz and Shafiee, 2018). Furthermore, they can form highly stable bioconjugates with common targeting biomolecules such as DNA and proteins (antibodies), similarly to what was observed in this study, thereby enabling highly specific and sensitive detection and sensing of viruses.

3.7.2. Raman measurement of glass substrates coated with various molecules

The HIV viral particle is spherical in shape and has a diameter of approximately 120 nm which is 60 times smaller than the size of a red blood cell (Otange et al., 2017; Freed, 1998; Mascarenhas and Musier-Forsyth, 2009; Farzin et al., 2020). The virus is surrounded by a phospholipid enveloped containing surface proteins; glycoprotein gp120 and glycoprotein gp41. On the inside, the virus has a cone shaped HIV-1 p24 antigen which is located on its core which is surrounded by a matrix composed of viral protein p17 (Farzin et al., 2020). It is expected that when the virus is excited, the Raman scattered radiation will consist of bands associated with the composition of the virus.

Fig. 9 shows the Raman spectra of glass substrates coated with HIV antibodies (no nanoparticles), AuNCs and SeNPs in the absence (no virus) and presence of the virus. The Raman spectra of anti-HIV gp41 antibodies immobilised on glass substrates in the presence and absence of the virus show similarities on certain Raman peaks; the vibration around the 900 cm^{-1} region which arises from the stretching mode of the N-C-C which is found in between peptide bonds. Similarly, the C-N stretching mode around 1100–1200 cm^{-1} region which can be attributed to the peptide bonds formed by the amino acids of the antibody and that of the virus. After the 1200 cm^{-1} point, vibrations from the amide III and C-H functional groups are observed on both the spectra. The differences in the samples are seen from the presence of the phenylalanine aromatic ring at 1000 cm^{-1} in the absence of the virus. Futhermore, the C-N mode is stronger in the absence of the virus compared to when the virus is present. In the presence of the virus, the aromatic rings of tyrosine, tryptophan and phenylalanine are present. The differences can be attributed to the random orientation that viral molecules take when they conjugate to the antibody. The results obtained show that the surfaces which were treated with the virus showed characteristic peaks that represent the carbohydrates of viral glycoprotein and proteins such as enzymes and lipids (Lee et al., 2015).

The spectra of AuNCs in the absence or presence of the virus show similarities in the spectra around the 1200 cm^{-1} region

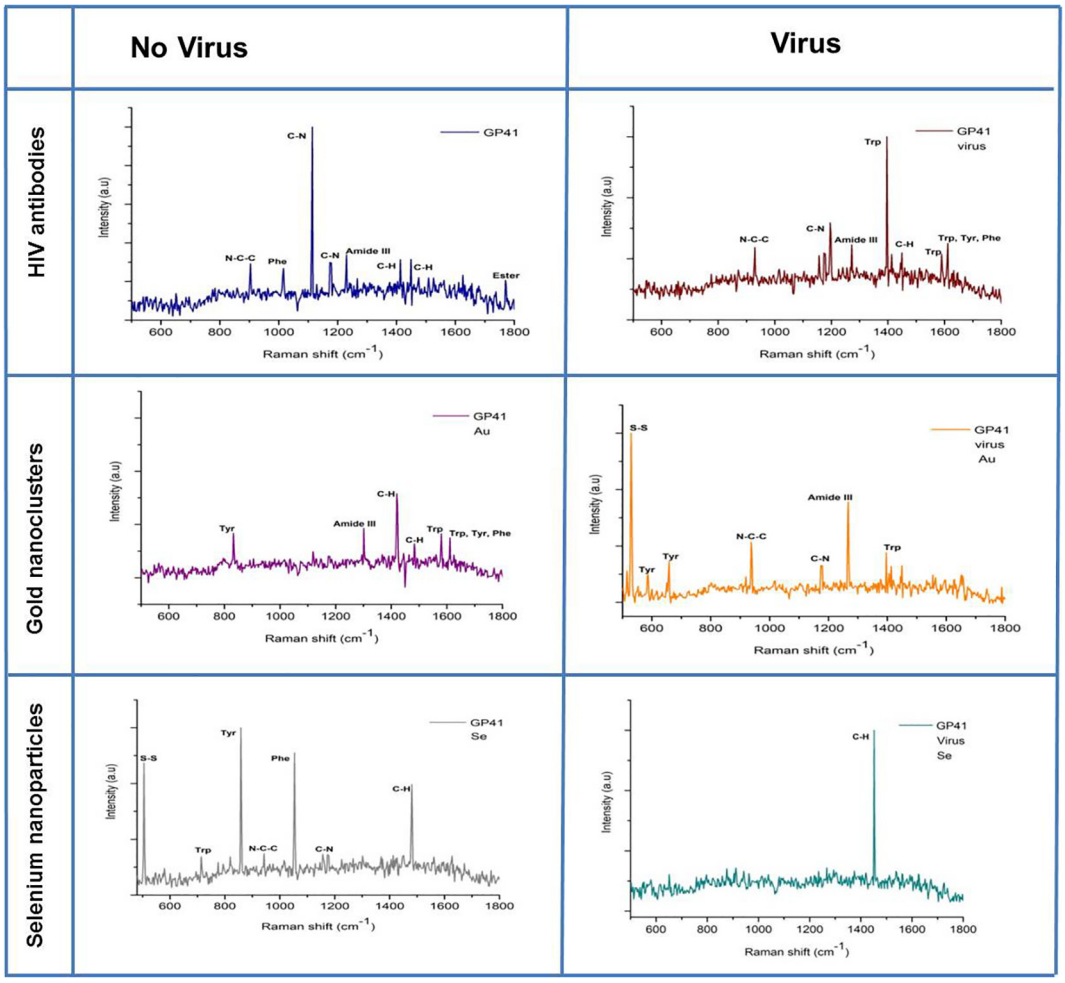

Fig. 9. Raman spectra of spectra glass substrates coated with HIV antibodies, gold nanoclusters conjugated to anti-HIV gp41 antibodies, selenium nanoparticle conjugated to anti-HIV gp41 antibodies in the absence (no virus) and presence of the virus (virus).

due the amide III vibration. In the absence of the virus, the aromatic amino acids (Tyr, Trp and Phe) are seen at 800 cm^{-1} and 1600 cm^{-1} region due to signal enhancement by the Au nanomaterial. In the presence of the virus, a sharp peak at 545 cm^{-1} arises due to disulphide bonds that are present in most proteins and viruses and this can indicate successful conjugation binding of the AuNPs to the virus. For the SeNPs, major differences are seen on the SeNPs in the absence of the HIV pseudoviruses. In the absence of the virus, the functional groups associated with amino acids are enhanced significantly compared to the viral sample. On the viral spectrum, only the C-H peak was observed and no clear peaks were observed.

The surface enhanced Raman spectroscopy (SERS) effects that takes place in the presence of nanoparticles are due to the coupling of the incident laser intensity with the localised surface plasmon resonance (LSPR) of the metal surfaces of nanoparticles which results in an enormous field enhancement which in turn enhances the Raman spectra of the analyte (Yang et al., 2017). The LSPR is caused by the oscillations of valence electrons in resonance with the incident light. Localisation is caused by the nanoparticles with the dimensions smaller than that of the wavelength and therefore crafting a locally amplified electromagnetic (EM) field which can be further enhanced in regions between nanoparticles because of near-field coupling (Yang et al., 2016). The scattering and absorption intensities of AuNPs are greater than identical sized non-plasmonic nanoparticles or semi-metallic nanoparticles because of the LSPR of AuNPs. This correlates with the LIF results obtained in this study, where the fluorescence intensity of AuNCs was superior as compared to SeNPs.

Nanoscale materials such as nanoparticles offer several advantages to biosensors and this includes; signal amplifications, sensitivity, specificity, selectivity, stability, rapidity and cost effectiveness (Farzin, et al., 2020; Oluwole et al., 2018). Detection of ultralow concentrations of biomarkers is impossible by using conventional Raman spectroscopy because the intensity of Raman scattering from the molecules is too low to be detected (Devi et al., 2015). However, when molecules are adsorbed on the surface of nanoparticle, particularly the plasmonic surface of the metal nanoparticles such as AuNCs used in this study, the intensity is highly enhanced by 10^8-10^{14} order of magnitude.

4. Conclusion

This study represents a proof of concept by using biosensors and nanomaterial as a reliable and potential tool for viral threat identification. In summary, we synthesized SeNPs and AuNCs, and both of these nanoparticles were successfully conjugated to anti-HIV g41 antibodies. The conjugated nanoparticles managed to bind to HIV pseudoviruses captured by anti-HIV g41 immobilized on the surface of glass substrates and this was confirmed by AFM. The method used in this study for immobilising antibodies

on the surface of a substrate and capturing of the analytes can be used in a variety of biosensing applications. The Raman spectroscopy results showed that the technique can be used for the detection of biomolecules on the surface of substrates and the method followed can be used to detect wide range of biological analytes. Further studies are required to determine the limit of detection of the system. Deploying nanomaterials was found to significantly improve the signal to noise ratio significantly and therefore adding to the sensitivity of the employed diagnostic biosensor. There is an urgent need of robust, affordable, sensitive and selective biosensors amid the global spread of viral threat and the fear of biological weapons. The same concept that was used in the current study could be used for the identification and quantification other viruses such as the COVID-19 which has results resulted in a global pandemic and overwhelming the health care systems in many countries. For the diagnosis of COVID-19 in clinical samples, the causative agent of the disease, severe acute respiratory syndrome coronavirus 2 (SARS-CoV-2) can be targeted. This will involve the immobilization of SARS-CoV-2 spike antibody on salinized glass substrates for capturing SARS-CoV-2 viruses. The sample to be tested can then be added to the substrates and the viruses will be captured by the immobilized antibody. Nanoparticles conjugated SARS-CoV-2 spike antibody can be added to the surface of the substrates for signal enhancement and improvement of the sensitivity of system. The same spectroscopic approach followed in the study can be adopted for the diagnosis of COVID-19. Future studies are required to validate this concept with COVID-19 and other viruses with the identification of the setup limit of detection, sensitivity and selectivity.

Declaration of Competing Interest

The authors declare that they have no known competing financial interests or personal relationships that could have appeared to influence the work reported in this paper.

Acknowledgements

The council for scientific and indusctrial research, Pretoria, South Africa, National Research Foundation, South Africa and African Laser Center, South Africa and the department of science and innovation of South Africa.

References

Ahmed, E., Marzouk, A., Harith, M., 2015. Discrimination between different crude oil grades using Laser induced break down spectroscopy. Spectrochim. Acta, Part B 113, 93–99.

Alonso, M.C., Trapiella-Alfonso, L., Fernandez, J.M.C., Pereiro, R., 2016. Functionalized gold nanoclusters as fluorescent labels for immunoassays: application to human serum immunoglobulin E determination. Biosensorrs Bioelectron. 77, 1055–1061.

Attia, Y.A., Vázquez- Vázquez, C., Blanco, M.C., Buceta, D., Arturo López-Quintela, M. A., 2016. Gold nanorod synthesis catalysed by Au clusters. Faraday Discuss. 191, 205–213.

Barre-Sinoussi, F., Cherman, J.C., Rey, F., Nugeyre, M.T., Chamaret, S., Gruest, J., Dauguet, C., Axler-Blin, C., Vezinet-Brun, F., Rouzioux, C., Rozenabaum, W., Montagnier, L., 1983. Isolation of a T-lymphotropic retrovirus from a patient at risk for acquired immune deficiency syndrome (AIDS). Science 220, 868–871.

Devi, R.V., Doble, M., Verma, R.S., 2015. Nanomaterials for early detection of cancer biomarker with special emphasis on gold nanoparticles in immunoassays/sensors. Biosens. Bioelectron. 68, 688–698.

Draz, M.S., Shafiee, H., 2018. Applications of gold nanoparticles in virus detection. Theranostics 8, 1985–2017.

El-Hussein, A., Manoto, S.L., Ombinda-Lemboumba, S., Alrowaili, Z.A., Mthunzi-Kufa, P., 2020. A review of chemotherapy and photodynamic therapy for lung cancer treatment. Anti-Cancer Agents Med. Chem. 18 (5), 438–1407.

El-Naggar, M.E., Shaheen, T.I., Fouda, M.M., Hebeish, A.A., 2016. Eco-friendly microwave-assisted green and rapid synthesis of well-stabilized gold and core-shell silver-gold nanoparticles. Carbohydr. Polym. 136, 1128–1136.

Farzin, L., Shamsipur, M., Samandari, L., Sheibani, S., 2020. HIV biosensors for early diagnosis of infection: the intertwine of nanotechnology with sensing strategies. Talanta 206, 120201.

Finetti, C., Sola, L., Pezzullo, M., Prosperi, D., Colombo, M., Riva, B., Avvakumova, S., Morasso, C., Picciolini, S., Chiari, M., 2016. Click chemistry immobilization on antibodies on polymer coated gold nanoparticles. Langmuir 32, 7435–7441.

Freed, E.O., 1998. HIV-1 gag proteins: diverse functions in the virus life cycle. Virology 251, 1–15.

Gardiner, D.J., Graves, P.R., 1989. Practical Raman spectroscopy. Springer.

Gotoshia, S.V., Gotoshia, L.V., 2008. Laser Raman and resonance Raman spectroscopies of natural semiconductor mineral cinnabar, α-HgS, from various mines. J. Phys. D Appl. Phys. 41, 115406.

Hausen, H., 2009. The search for infectious causes of human cancers: where and why. Virology 15, 1–10.

Ignat, T., Miu, M., Kleps, I., Bragaru, A., Simion, M., Danila, M., 2010. Electrochemical characterization of BSA/11-mercatoundecanoic acid on Au electrode. Material Science and Engineering B. 169, 55–61.

Jazayeri, M.H., Amani, H., Pourfatollah, A.A., Pazoki-Toroudi, H., Sedighimoghaddam, B., 2016. Various methods of gold nanoparticles (GNPs) conjugation to antibodies. Sens. Bio-Sens. Res. 9, 17–22.

Jiang, J., Oberdorster, G., Biswas, P., 2009. Characterization of size, surface charge, and agglomeration state of nanoparticle dispersions for toxicological studies. J. Nanopart. Res. 11, 77–89.

Jin, R., 2010. Quantum sized, thiolate-protected gold nanoclusters. Nanoscale 2, 343–362.

Khalid, A., Tran, P., Norello, R., Simpson, D., O'Connor, A.J., Tomljenovic-Hanic, S., 2016. Intrinsic fluorescence of selenium nanoparticles for cellular imaging applications. Nanoscale 8, 3376–3385.

Krishnan, K.S., Raman, C.V., 1928. The negative absorption of radiation. Nature 122, 12–13.

Lee, J., Kim, B., Oh, B., Choi, J., 2015. Highly sensitive electrical detection of HIV virus based on scanning tunnelling microscopy. J. Nanosci. Nanotechnol. 15, 1117–11112.

Link, S., El-Sayed, M.A., 2003. Optical properties and ultrafast dynamis of metallic nanocrystals. Ann. Rev. Phys. Chem. 54, 331–366.

Lugongolo, M.Y., Manoto, S.L., Ombinda-Lemboumba, S., Mthunzi-Kufa, P., 2017. The effects of low level laser therapy on both HIV-1 infected and unifected TZM-bl cells. J. Biophotonics 10, 1335–1344.

Malabi, R., Manoto, S.L., Ombinda-Lemboumba, S., Maaza, M., Mthunzi-Kufa, P., 2019. Laser-enhanced drug delivery of antiretroviral drugs into human immunodeficiency virus-1 infected TZMbl cells. J. Biophotonics 12, e201800424.

Manoto, S.L., Lugongolo, M., Govender, U., Mthunzi-Kufa, P., 2018. Point of care diagnostics for HIV in resource limited settings: an overview. Medicina 54, 1–14.

Manoto, S.L., Mabena, C., Malabi, R., Ombinda-Lemboumba, S., El-Hussein, A., Kasem, M., Mthunzi-Kufa, P., 2020. Smartphone biosensing for point of care diagnostics. Frontiers in Biological Detection: From Nanosensors to Systems XII vol. 11258, p. 112580J.

Mascarenhas, A.P., Musier-Forsyth, K., 2009. The capsid protein of human immunodeficiency virus: interactions of HIV-1 capsid with host protein factors. FEBS J. 21, 6118–6127.

Nguyen, T., Bang, D.D., Wolff, A., 2020. 2019 novel coronavirus disease (COVID-19): paving the road for rapid detection and point-of-care diagnostics. Micromachines 11 (3), 306.

Oliveira, J.P., Prado, A.R., Keijok, W.J., Antunes, P.W.P., Yapuchura, E.R., Guimaraes, M.C.C., 2019. Impact of conjugates strategies for targeting of antibodies in gold nanoparticles for ultrasensitive detection of 17 β-estradiol. Sci. Rep. 9, 13859.

Oluwole, D.O., Manoto, S.L., Malabi, R., Maphanga, C., Ombinda-Lemboumba, S., Mthunzi-Kufa, P., Nyokong, T., 2018. Evaluation of the photophysicochemical properties and photodynamic therapy activity of nanoconjugates of zinc phthalocyanine linked to glutathione capped Au and Au3Ag1 nanoparticles. Dyes Pigm. 150, 139–150.

Otange, B., Birech, Z., Rop, R., 2017. Conductive silver paste smeared glass substrates for label-free Raman spectroscopic detection of HIV-1 and HIV-1 p24 antigen in blood plasma. Anal. Bioanal. Chem. 409, 3253–3259.

Puertas, S., Batalla, P., Moros, M., Polo, E., Del Pino, P., Guisan, J.M., Grazu, V., De la Fuente, J.M., 2011. Taking advantage of unspecific interactions to produce highly active magnetic nanoparticle-antibody conjugates. ACS Nano 5, 4521–4528.

Qu, X., Li, Y., Li, L., Wang, Y., Liang, J., Liang, J., 2015. Fluorescent gold nanoclusters: synthesis and recent biological application. J. Nanomater. 2015, 1–23. https://doi.org/10.1155/2015/784097.

Singhvi, J.G., 2019. Multifunctional nanocrystals for cancer therapy: a potential nanocarrier. Nanomater. Drug Deliv. Therapy 2019, 91–116.

Souad Elfeky, A., El-Hussein, A., 2018. Photostability study of CdTe quantum dots using laser induced fluorescence. In: Proc. SPIE 10711, Biomedical Imaging and Sensing Conference, pp. 1071128.

Sonawane, M.D., Nimse, S.B., 2016. Surface modification chemistries of materials used in diagnostic platforms with biomolecules. J. Chem., 1–19

Su, H., Li, S., Jin, Y., Xian, Z., Yang, D., Zhou, W., Mangaran, F., Leung, F., Sithamparanahan, G., Kerman, K., 2017. Nanomaterial based biosensors for biological detections. Adv. Helath Care Technol. 3, 19–29.

UNAIDS. Fact sheet-world AIDS day 2019. Global HIV statistics. https://www.unaids.org/sites/default/files/media_asset/UNAIDS_FactSheet_en.pdf.

Vahdati, M., Moghadam, T., 2020. Synthesis and characterization of selenium nanoparticles-lysozyme nanohybrid system with synergistic antibacterial properties. Sci. Rep. 10, 510.
Virgin, H.W., 2014. The virome in mammalian physiology and disease. Cell 157 (1), 42–50.
Wang, Z., Jing, J., Ren, Y., Guo, Y., Tao, N., Zhou, Q., Zhang, H., Ma, Y., Wang, Y., 2019. Preparation and application of selenium nanoparticles in a lateral flow immunoassay for clebuterol detection. Mater. Lett. 234, 212–215.
Wang, S., Meng, X., Das, A., Li, T., Song, Y., Cao, T., Zhu, X., Zhu, M., Jin, R., 2014. A 200-fold quantum yield boost in the photoluminescence of silverdoped Ag_xAu25_x nanoclusters: the 13th silver atom matters. Angewandte Commun. 53, 2376–2380.
Welch, N.G., Scoble, J.A., Muir, B.W., Pigram, P.J., 2017. Orientation and characterization of immoboilized antibodies for improved immunoassays. Biointerphases 12, 02D301.
Yang, G., Nanda, J., Wang, B., Chen, G., Hallinan, D.T., 2017. Self-assembly of large gold nanoparticles for surface-enhanced Raman spectroscopy. ACS Appl. Mater. Interfaces 9, 13457–13470.
Yang, G., Hu, L., Keiper, T.D., Xiong, P., Hallinan, D.T., 2016. Gold nanoparticle monolayers with tunable optical and electrical properties. Langmuir 32, 4022–4033.
Yu, Q., Gao, P., Zhang, K., Tong, X., Yang, H., Liu, S., Du, J., Zhao, Q., Huang, W., 2017. Luminescent gold nanocluster-based sensing platform for accurate H2S detection in vitro and in vivo with improved anti-interference. Light Sci. Appl. 6, e17107.
Zhang, Z., Guo, Q., Cui, D., 2009. Recent Advances in nanotechnology applied to biosensors. Sensors 9, 1033–1053.
Zhao, V.X.T., Wong, T.I., Zheng, X.T., Tan, Y.N., Zhou, X., 2020. Colorimetric biosensors for point of care virus detections. Mater. Sci. Energy Technol. 3, 237–249.